Supporting Information

Anion Exchange on Surface Induces Drastic Fluorescence Response in Cu(II) Coordination Polymer Crystals

Lu Huang, Hongyuan Cheng, Luxi Wang, Xiaojing Wu and Bo Qin*

College of Chemistry and Chemical Engineering, Chongqing University, Chongqing, 401331, China.

E-mail: qinbo@cqu.edu.cn

Experimental Details

1. Materials

All reagents were obtained from commercial suppliers and used as received specified. Aqueous solutions were prepared from distilled water. Reactions were monitored by thin-layer chromatography (TLC) on silica gel pre-coated glass plate. Chemical yields refer to pure isolated substances.

2. Apparatus and measurements

Mass spectra were obtained using the Instrumentation include Finnigan MAT95XL-T and Micromass VG7035. ^{1}H NMR spectra were recorded on Agilent DD2600 (600 MHz) or Agilent DD2400 (400 MHz) spectrometers. The solvent signal of $CDCl_3$ was referenced at δ = 7.26 ppm, and DMSO-d_6 at 2.50

ppm. Coupling constants (*J* values) were reported in Hertz (Hz). ^{1}H NMR data were recorded in the order: chemical shift value, multiplicity (s, singlet; d, doublet; t, triplet; q, quartet; m, multiplet; br, broad), number of protons that gave rise to the signal and coupling constant, where applicable. ^{13}C spectra were proton-decoupled and recorded on Agilent DD2600 (600 MHz). The solvent, $CDCl_3$ was referenced at 77 ppm and DMSO-d_6 at 39.5 ppm. Powder X-ray diffraction (PXRD) data were collected on a SHIMADZU X ray diffractometer XRD-6000, using Cu-Kα radiation (λ=1.5406 Å). Solid-state fluoroscence spectra were recorded on Fluorolog-3 spectrofluorometer (Horiba JobinYvon) with a 450 W Xenon Lamp as the excitation source and a picosecond photon detection module (PPD-850, Horiba Scientific) as the detector. The UV-vis absorption spectra was carried on a Shimadzu UV-3600 spectrophotometer. X-ray single crystal diffractometer date were recorded on a Agilent SuperNova Dual diffractometer using Cu-Kα (λ=1.54184Å). The scanning electron microscopy (SEM) images were obtained on JSM-7800F scanning electron microscope. The transmission electron microscopy (TEM) and TEM mapping images were performed by Tecnai G2 20 S-Twin transmission electron microscope. The anion chromatography data were obtained on IC-2010. Pyrolysis thermogravimetric analysis (TG), and differential thermal analysis (DTA) were performed using a Mettler Toledo TGA/DSC1/1600LF thermal analysis system. The samples (1.5 mg) were heated from room temperature, followed by dynamic heating to 800 °C at a heating rate of 10 °C

min^{-1}. Nitrogen was passed through the furnace at a flow rate of 50 mL min^{-1}. X-ray photoelectron spectroscopy (XPS) measurements were performed with an ESCALAB250Xi instrument.

3 Synthesis and anion exchange

3.1 Synthesis of the ligand L

Diethyl 4-oxo-1,4-dihydropyridine-3,5-dicarboxylate (**a**) and diethyl 1-benzyl-4-oxo-1,4-dihydropyridine-3,5-dicarboxylate (**b**) were prepared according to literature procedures.[1]

*1-benzyl-4-oxo-1,4-dihydropyridine-3,5-dicarboxylic acid (**c**)*

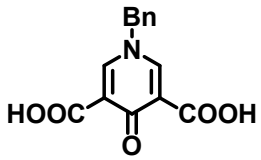

c

Compound **b** (6.58g, 20.0 mmol) was dissolved in ethanol (80 mL), to which 1M KOH (80 mL, 80.0 mmol) was added at room temperature. The mixture was allowed to stir at 60℃ for 4 hours. Then ethanol was removed in vacuo and the aqueous layer was acidated by addition of 1M HCl to pH=4-5. The precipitated crude product was collected by filtration and dried in the oven, which was recrystallized from methanol to give the pure product 3 as a white solid. Yield: 5.28 g, 97%. ^{1}H NMR (400 MHz, DMSO-d_6) δ 14.26 (s, 2H), 8.92 (s, 2H), 7.47 – 7.43 (m, 3H), 7.42 – 7.37 (m, 2H), 5.51 (s, 2H). ^{13}C NMR (100 MHz, DMSO-d_6) δ 176.43, 164.12, 147.66, 135.12, 129.08, 128.81, 128.29, 118.80, 59.97, HRMS-EI: calculated for $[M+H]^+$ ($C_{14}H_{11}NO_5$): *m/z* 274.0715, found: *m/z* 274.0716.

*1-benzyl-4-oxo-N^3,N^5-bis(pyridin-4-ylmethyl)-1,4-dihydropyridine-3,5-dicarboxamide (**L**) synthesis*

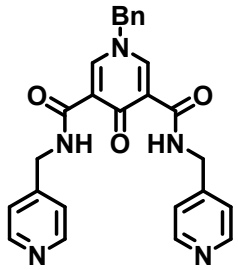

L

Acid **c** (3.00 g, 11.0 mmol) and BOP (9.71 g, 22.0 mmol) were dissolved in CH_2Cl_2 (30 mL) to which DIEA (7.28mL, 44mmol) was added at 0^0C. The reaction mixture was stirred for at least 15 mins then a solution of N-Methyl-4-pyridinamine (2.68 ml, 26.4 mmol) was added. The reaction mixture was allowed to stir continuously 12 hours at room temperature. The reaction mixture was washed with water (3*50ml). The organic phase in the filtrate was collected, drying over Na_2SO_4 and removal of solvent in vacuo gave the crude product, which was recrystallized from methanol to give the pure product **L** as a white wadding solid. Yield: 3.10g, 63%. ^{1}H NMR (600 MHz, $CDCl_3$) δ 10.42 (s, 1H), 8.67 (s, 1H), 8.55 (d, J = 5.7 Hz, 2H), 7.43 – 7.41 (m, 1H), 7.25 (s, 1H), 5.16 (s, 1H), 4.64 (d, J = 6.0 Hz, 2H). ^{13}C NMR (150 MHz, $CDCl_3$) δ 176.34, 163.73, 149.94, 147.31, 145.06, 133.09, 129.70, 129.65, 127.89, 122.16, 121.81, 77.24, 77.03, 76.82, 62.01, 42.19, HRMS-EI: calculated for $[M+H]^+$ ($C_{26}H_{24}N_5O_3$): *m/z* 454.1879, found: *m/z* 454.1878.

3.2 Synthesis of 1⊃F^-, 1⊃NO_3^-, 1⊃Cl^-, and 1⊃Br^-

Cu(II)-Pyridyl ketone complexes were prepared according to reaction of CuX_2 (X=F^-, Cl^-, Br^-, NO_3^-)(0.5 mmol) with ligand **L** (1 mmol) in 25ml water with 110^0C for 4 hours, then rinsed with water for 4-5 times and vacuum dried to obtain solid powder.

3.3 Anion Exchange reactions

Powder of **1⊃F^-** (0.2 mmol) were separately added in 10ml water solutions with

$NaNO_3$, NaCl and NaBr (2 mmol) at 110^0C for 1h , then rinsed with water for 4-5 times and vacuum dired, which obtained the anion-exchanged product **1⊃F^-&NO_3^-**, **1⊃F^-&Br^-** and **1⊃F^-&Cl^-**. The same method and procedure could obtain other anion exchange products.

4 X-ray Crystallographic Analysis

Single crystals suitable for X-ray diffraction analysis were obtained for complexes **1⊃NO_3^-** from water/N,N-Dimethylformamide(2:1). Single-crystal X-ray data of compound **1⊃NO_3^-** were collected at 120 K. Using Olex2,[2] the structure was solved with the XM[3] structure solution program using Dual Space and refined with the ShelXL[4] refinement package using Least Squares minimisation. Details of the X-ray structure determinations and refinements are provided in Table S1 for **1⊃NO_3^-**.

5. Density function theory (DFT) calculation

In this study, the DFT calculations were performed using the Gaussian 03 and the DMol3 software package. The interaction on energy of the complex was calculated as $\Delta E=E_n-E_a$ by Gaussian 03 at the M062X/6-311++g (d,p) level. Here, E_n and E_a represent the energy of the two ligands being close to and away from each other, respectively. A local-density approximation (LDA) of the Perdew-Wang (PWC) was employed to describe electronic transfer. All Electron approximation was utilized with the double numerical plus polarization (DNP) basis set. The convergence tolerance of energy was taken as 1×10^{-5} Hartree.

Supplementary Data

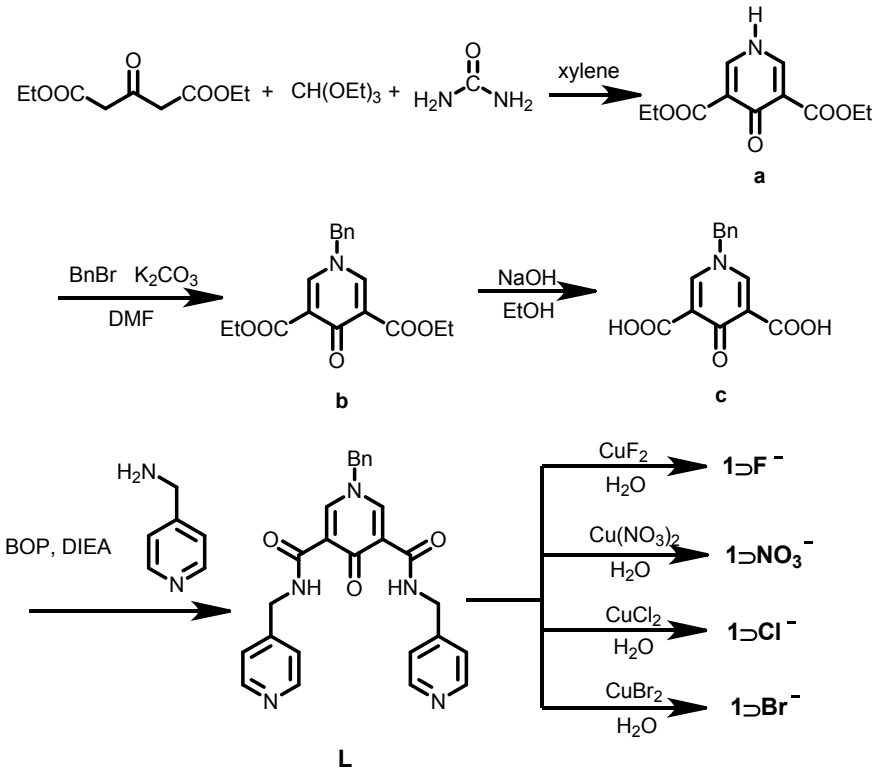

Scheme S1. Synthesis route of **L** and **1⊃X⁻**

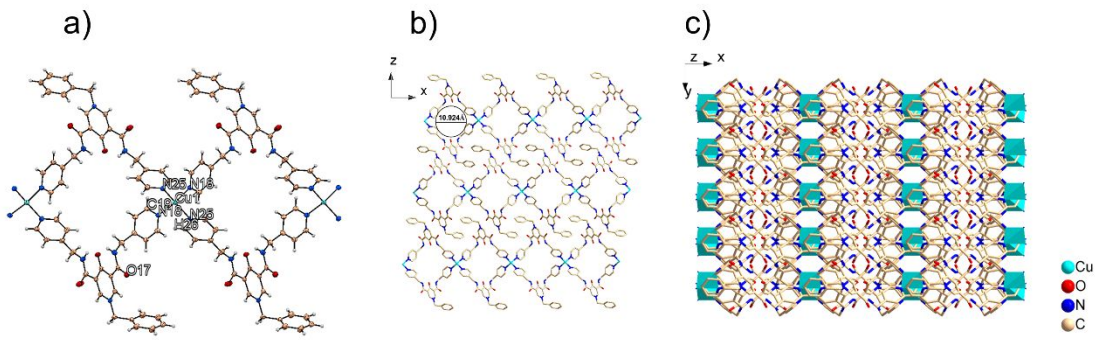

Figure. S1. (a)Crystal structure of **1⊃NO_3^-**, NO_3^- exist as free ions in the cavity. (b) 2D planar sheet in **1⊃NO_3^-**. (c) Side view of **1⊃NO_3^-**. Atoms are represented by colored as O: red, C: light gray, Cu: cyan, N: blue, H: dark gray, and hydrogen atoms were omitted for clarity in (b) and (c).

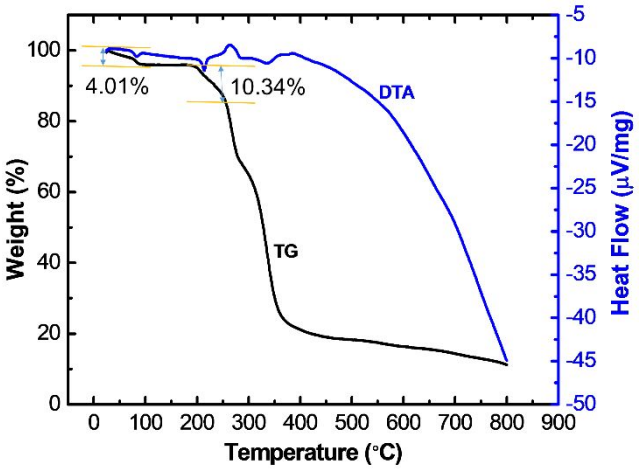

Figure. S2. TG curves of **1⊃NO_3^-**.

The loss of 3 free water with a mass loss of 4.01% is a first stage reaction in the temperature range of 25–100℃. The second stage loss of 7 crystalline water with a mass loss of 10.34%, which occurs in the temperature range of 187–252℃. The calculation method assumes that the number of water molecules was *A*, and used the amount of ligand and copper nitrate (1093) to calculate

the number. The number of water (A=10) was calculated on the basis of equation 1:

$$\frac{18A}{1093 + 18A} = 14.35\%$$

In addition, suppose the number of free water was x and the number of crystal water was y. x+y=10, x/y=4.01/10.34, getting the number of free water was 3 and the number of crystal water was 7.

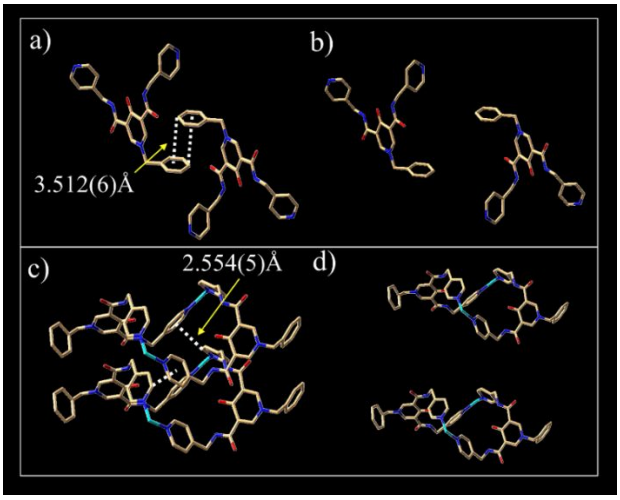

Figure. S3 (a) The model of the π-π stacking interaction between the benzenes in the complex. (b) The model without the π-π stacking interaction. (c) The model of the CH-π interaction between the pyridyl-pyridyl rings stack between the layers. (d) The model without the CH-π stacking interaction.

5 Spectroscopy

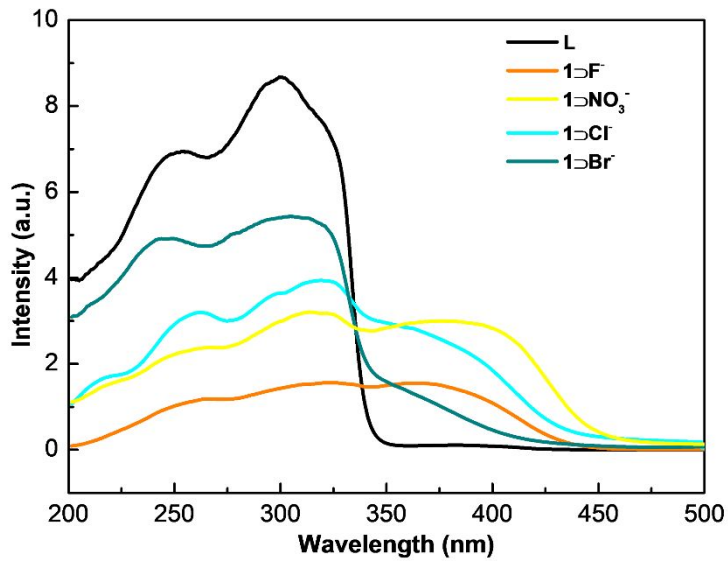

Figure. S4 Diffuse reflectance UV-visible (UV-vis) spectroscopy of the **L**, **1⊃F**$^-$, **1⊃NO**$_3^-$, **1⊃Cl**$^-$ and **1⊃Br**$^-$.

Ligand **L** has two absorption bands, respectively. The 225-275 nm absorption band is π-π* transition, and the 275-325 absorption band is n-π* transition. There is an absorption band between 350-425 nm because of the d-d transition in the ligand field absorption band formed by ligand coordination with Cu ion.

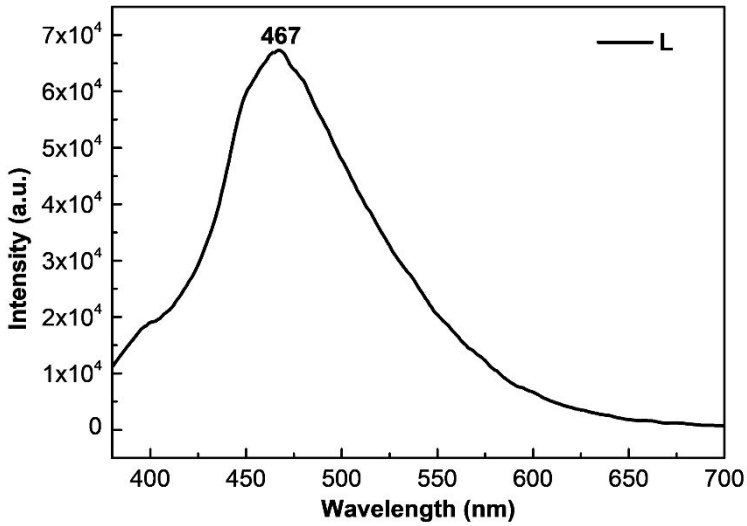

Figure. S5. Solid-state luminescence spectrum of **L** (λ_{ex} = 366 nm).

5 Anion exchange learning

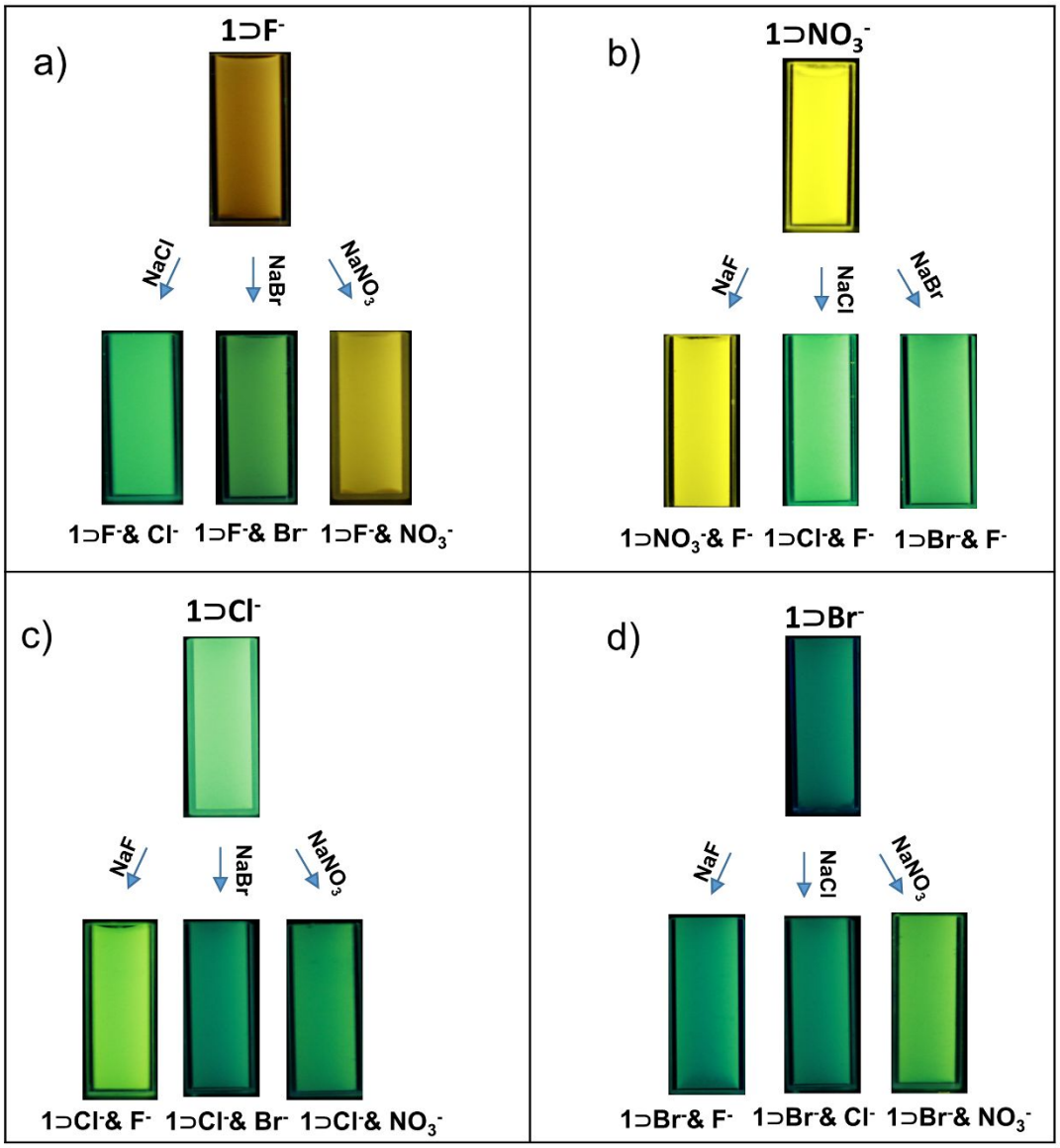

Figure. S6. Photographs showing **1⊃F⁻**, **1⊃NO_3^-**, **1⊃Cl⁻**, and **1⊃Br⁻** and their various anion-exchanged products under UV irradiation with black light (365 nm). (a) Photograph of 10 equivalent other anions (NO_3^-, Cl^-, Br^-) added to **1⊃F⁻**. F^- ions can be replaced by all other anions. (b) Photograph of 10 equivalent other anions (F^-, Cl^-, Br^-) added to **1⊃NO_3^-**.

NO_3^- anion cannot be replaced by F^-, but can be replaced by Cl^- and Br^-. (c) Photograph of 10 equivalent other anions (F^-, NO_3^-, Br^-) added to **1⊃Cl⁻**. Cl^- anion can be replaced by Br^-, but cannot be replaced by F^- and NO_3^-. Fluorescence intensity is the main basis to distinguish whether Cl^- anion is replaced by Br^-. (d) Photograph of 10 equivalent other anions (F^-, NO_3^-, Cl^-) added to **1⊃Br⁻**. Br^- anion cannot be replaced by other anions. But NO_3^- can partly replace Br^-.

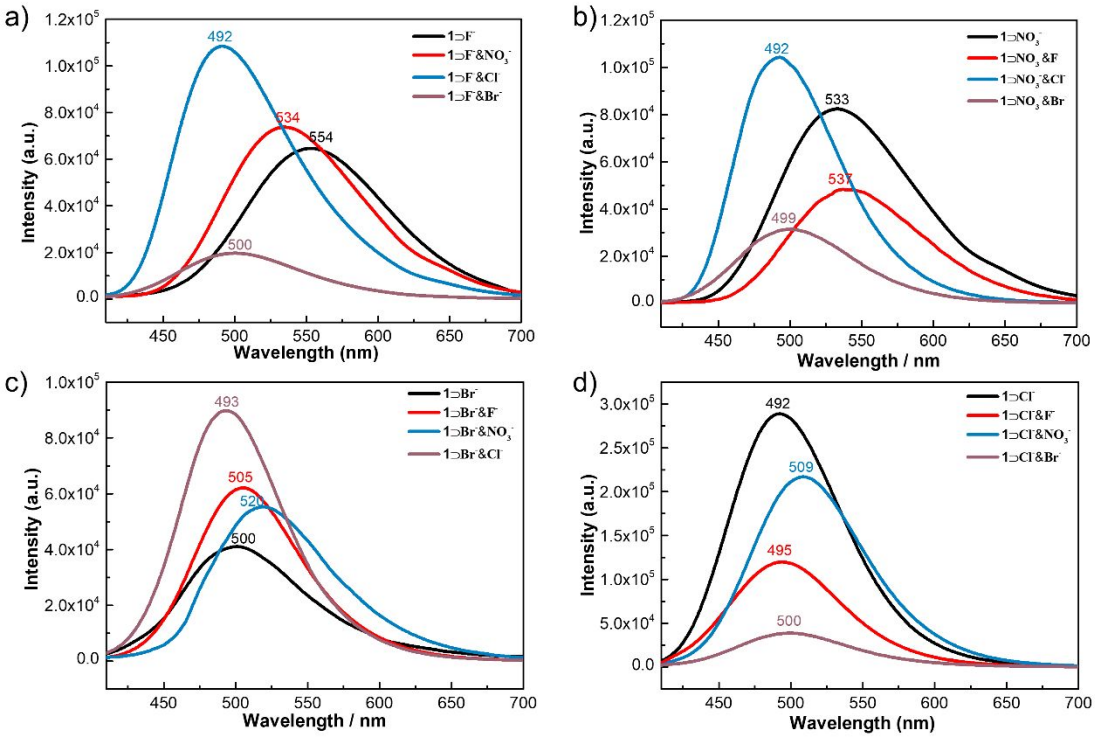

Figure. S7. Solid-state luminescence spectra of **L-CuX$_2$** (X=F^-, NO_3^-, Cl^-, Br^-) and their various anion-exchanged products. They were the fluorescence spectrums of the corresponding substances in Figure. S7.

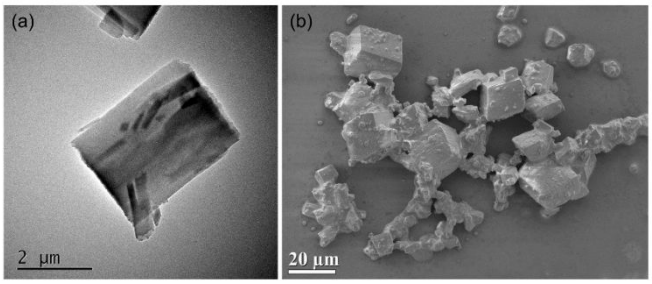

Figure. S8. (a) **TEM** images of **1⊃NO_3^-&Cl^-** after ultrasonic treatment in aqueous for 1 hour at room temperature. After adding NaCl to **1⊃NO_3^-**, the structure of matter has no significant change in macroscopic structure. (b) **SEM** images of **1⊃NO_3^-&Cl^-**, show that **1⊃NO_3^-&Cl^-** structures are saved in sheets, and eventually form blocks like **1⊃NO_3^-** structures by stacking.

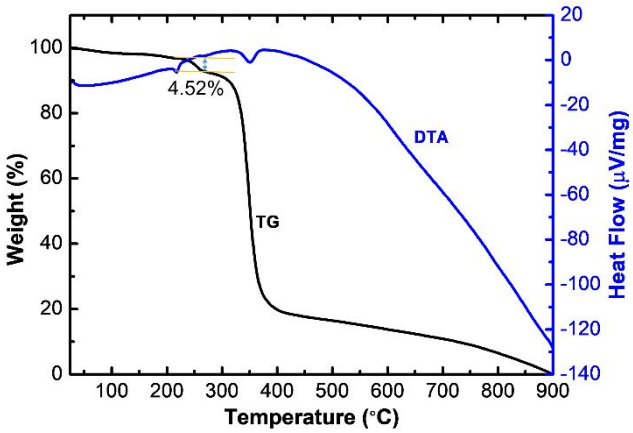

Figure. S9. TG curves of **1⊃NO_3^-&Cl^-**. Loss of 3 crystalline water of **1⊃NO_3^-&Cl^-** with a mass loss of 4.52%, which occurs in the temperature range of 231–272℃, and as temperatures continue to rise, the **1⊃NO_3^-&Cl^-** skeleton begins to collapse at 325℃.

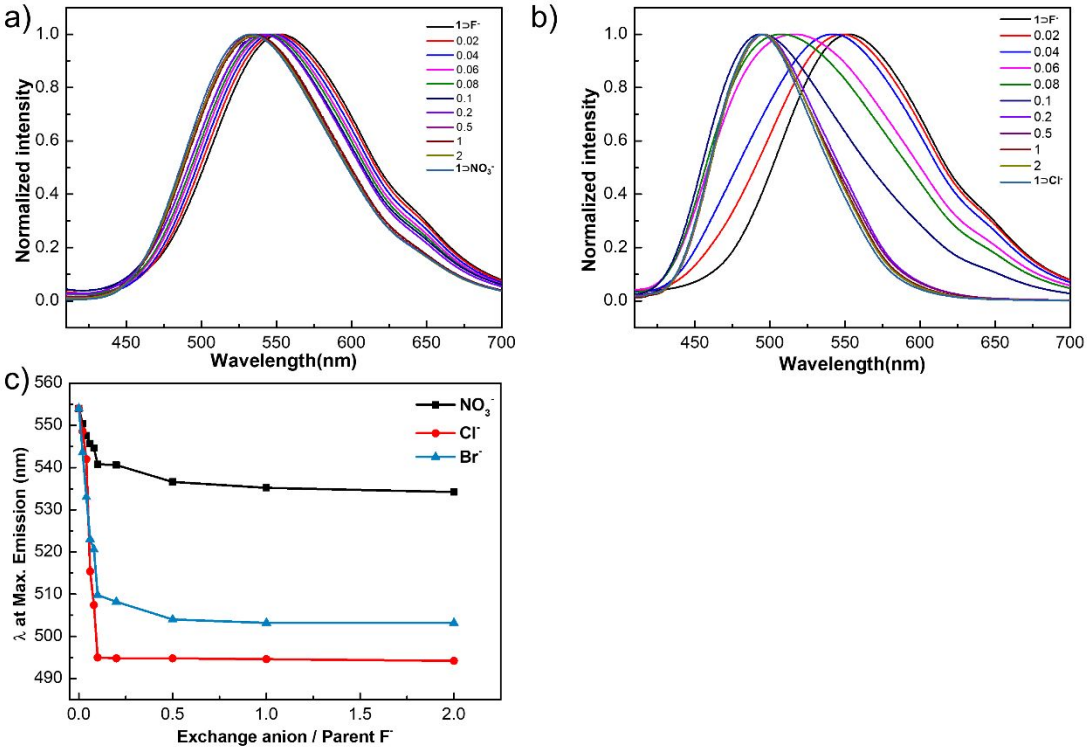

Figure. S10. Evolution of Solid-state emission spectra of the anion exchange reaction of **1⊃F⁻** with other anions at different reaction equivalents relative to F^- (a) NO_3^-, (b) Cl^-. (c) Maximum emission wavelength of various equivalent NO_3^-, Cl^- and Br^- anions added to **1⊃F⁻** at the excitation of 366 nm.

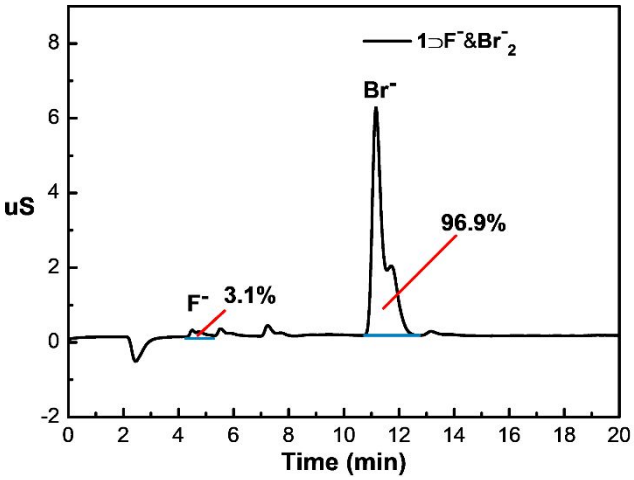

Figure. S11. Anion chromatogram of **1⊃F⁻&Br^-_2**. The contents of F^- and Br^- in the **1⊃F⁻**

&Br_2 were 3.1% and 96.9%, respectively.

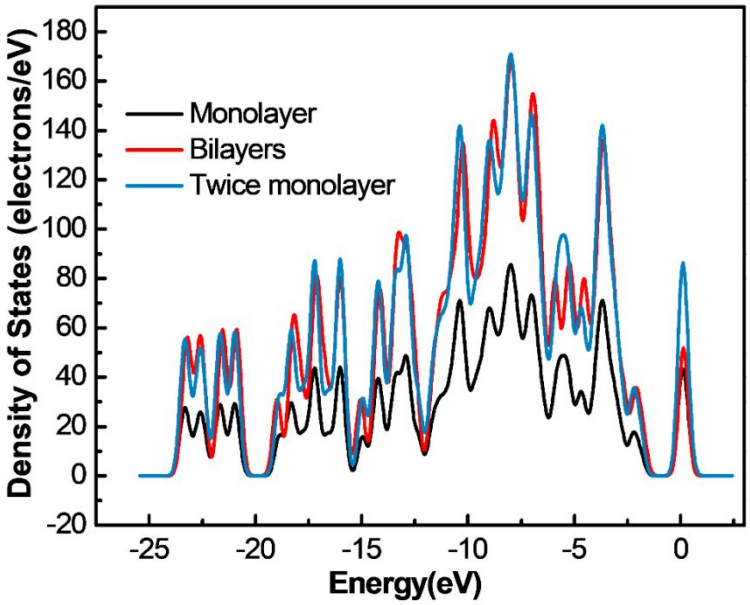

Figure. S12. Solid Density of states of the monolayer and bilayer of Cu (II)-CPCs calculated by the DMol3 functional.

Using the density functional theory (DFT), we computed the density of states (DOS) of Cu(II)-CPCs to shed some additional insights into the anion exchange-induced changes in emission wavelength. The idea behind these computations is that both intra- and inter-layer electrons transfer. In general, when electrons transfer between inter-layer, the charge will be redistributed, the contribution of each atom to DOS is different, which will change greatly.[5] The computed DOS of Cu(II)-CPCs showed that, despite of great similarity in peak position and shape, the strength of the bilayers is about twice that of the monolayers in Cu(II)-CPCs suggesting the inter-layer electron transfer to be very difficult.[6] A possible reason is that the chains and layers of Cu(II)-CPCs

are linked by non-covalent bonds.

Table S1. Crystal data and refinement parameters of **1⊃NO_3^-**

Identification code	gx-0704-120k
Empirical formula	$C_{104}H_{92}Cu_2N_{20}O_{12}$
Formula weight	1941.05
Temperature/K	120.00(10)
Crystal system	monoclinic
Space group	P2/c
a/Å	12.8724(2)
b/Å	5.50330(10)
c/Å	34.3016(6)
α/°	90
β/°	99.404(2)
γ/°	90
Volume/$Å^3$	2397.29(7)
Z	1
ρ_{calc}g/cm^3	1.345
μ/mm^{-1}	1.145
F(000)	1010.0
Crystal size/mm^3	0.22 × 0.18 × 0.15
Radiation	CuKα (λ = 1.54184)

2Θ range for data collection/°	6.96 to 142.734
Index ranges	$-15 \leq h \leq 11$, $-4 \leq k \leq 6$, $-42 \leq l \leq 39$
Reflections collected	8644
Independent reflections	4528 [R_{int} = 0.0279, R_{sigma} = 0.0366]
Data/restraints/parameters	4528/0/312
Goodness-of-fit on F^2	1.049
Final R indexes [I>=2σ (I)]	R_1 = 0.0373, wR_2 = 0.0976
Final R indexes [all data]	R_1 = 0.0436, wR_2 = 0.1007
Largest diff. peak/hole / e $Å^{-3}$	0.37/-0.35

Table S2. The radius and hydration free energies of anions[7]

Anion	Ion radius(Å)	$\Delta G_{hydration}$/(kJ/mol)	Hydrated radius(Å)
F^-	1.36	-429	3.52
NO_3^-	1.79	-300	3.40
Cl^-	1.81	-304	3.32
Br^-	1.95	-277	3.30

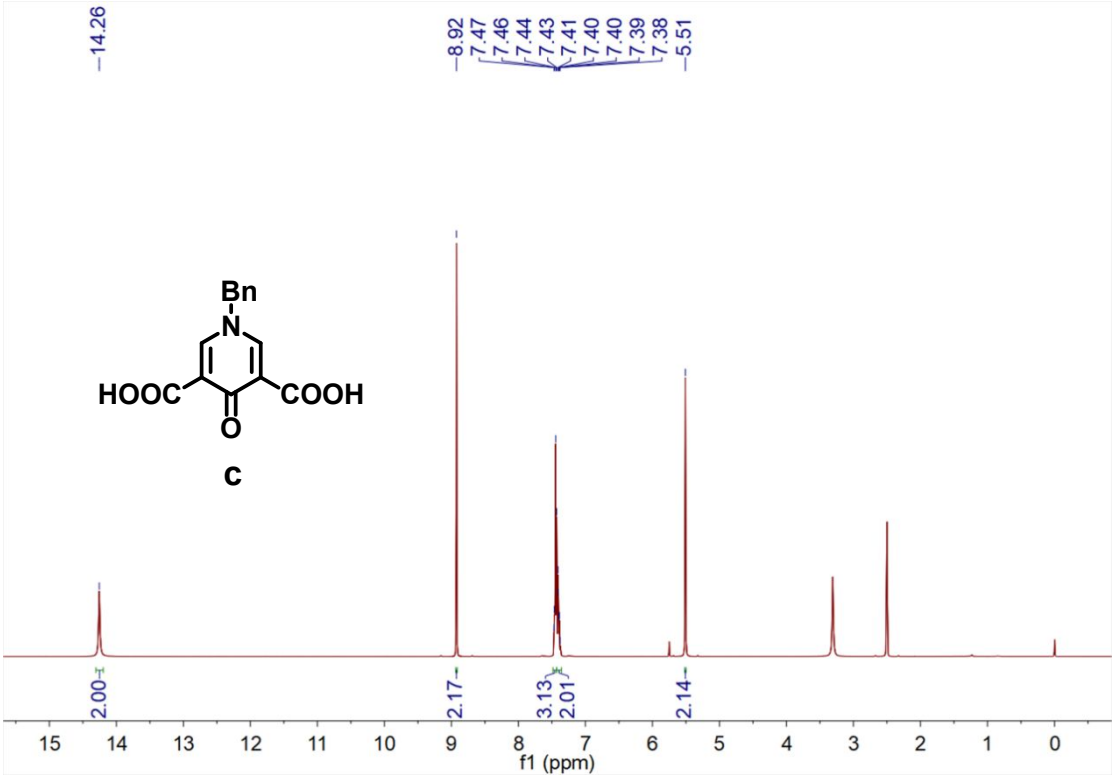

Figure. S13. ^{1}H NMR (400 MHz) spectrum of compound **c** in DMSO-d_6.

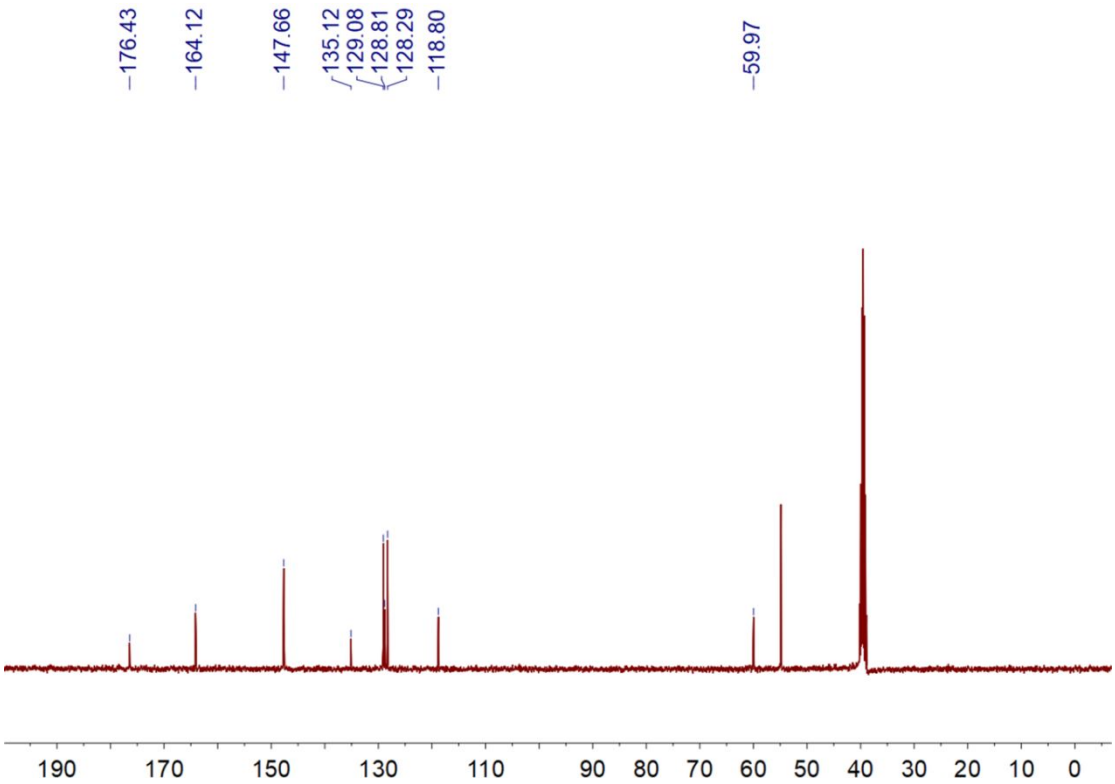

Figure. S14. ^{13}C NMR (100 MHz) spectrum of compound **c** in DMSO-d_6.

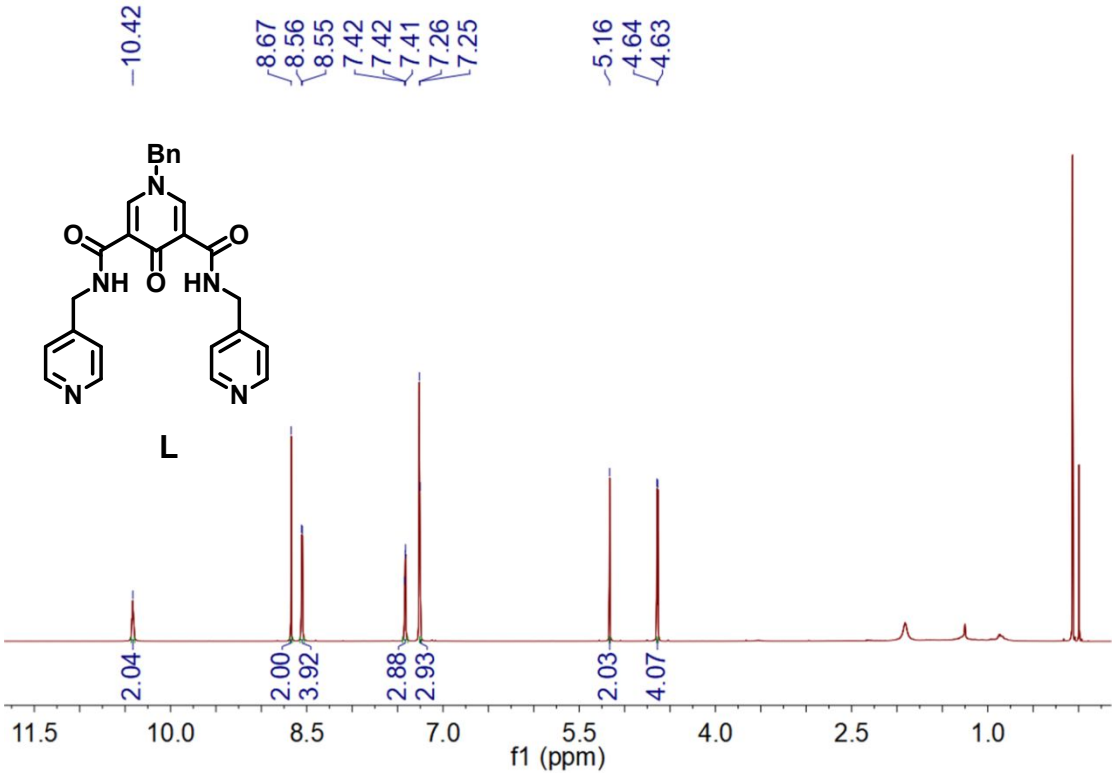

Figure. S15. ^{1}H NMR (600 MHz) spectrum of compound **L** in $CDCl_3$.

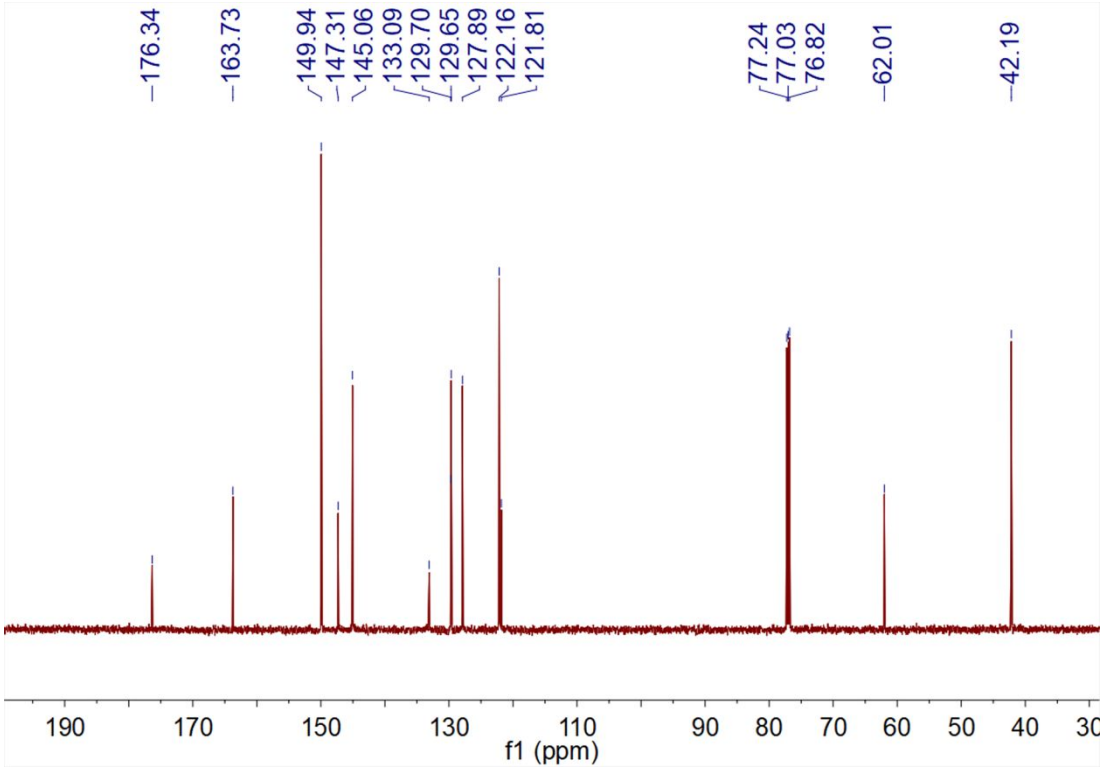

Figure. S16. ^{13}C NMR (150 MHz) spectrum of compound **L** in $CDCl_3$.

References

1. (a)Zheng, S. J.; J. Thompson, D.; Tontcheva, A.; Khan, S. I.; Rubin, Y. Perchloro-2,5,8-triazaphenalenyl Radical. *Org. Lett.* **2005**, *7,* 1861-1863. (b) Ren, C. L.; Maurizot, V.; Zhao, H. Q.; Shen, J.; Zhou, F.; Ong, W. Q.; Du, Z. Y.; Zhang, K.; Su, H. B.; Zeng, H. Q. Five-Fold-Symmetric Macrocyclic Aromatic Pentamers: High-Affinity Cation Recognition, Ion-Pair-Induced Columnar Stacking, and Nanofibrillation. *J. Am. Chem. Soc.* **2011**, *133,* 13930-13933.
2. Dolomanov, O. V.; Bourhis, L. J.; Gildea,R. J.; Howard, J. A. K.; Puschmann, H. OLEX2: a complete structure solution, refinement and analysis program. *J. Appl. Cryst.* **2009**, *42,* 339-341.
3. (a) Sheldrick, G. M. *Acta Cryst.* **2008**, A64, 112-122; (b) Sheldrick, G. M.;

Acta Cryst. **2015**, *C71,* 3-8.

4. Beer, P. D.; Gale, P. A. Anion Recognition and Sensing: The State of the Art and Future Perspectives. *Angew. Chem. Int. Ed.* **2001**, *40*, 486-516.
5. Dolgopolova, E. A.; Brandt, A. J.; Ejegbavwo, O. A.; Duke, A. S.; Maddumapatabandi, T. D.; Galhenage, R. P.; Larson, B. W.; Reid, O. G.; Ammal, S. C.; Heyden, A.; Chandrashekhar, M.; Stavila, V.; Chen, D. A.; Shustova, N. B. Electronic Properties of Bimetallic Metal-Organic Frameworks (MOFs): Tailoring the Density of Electronic States through MOF Modularity. *J. Am. Chem. Soc.* **2017**, *139*, 5201-5209.
6. Pratik, S. M.; Gagliardi, L.; Cramer, C. J. Boosting Photoelectric Conductivity in Porphyrin-Based MOFs Incorporating C_{60}. *J. Phys. Chem. C* **2019**, *124,* 1878-1887.
7. (a) Li, J.; Wang, F. Accurate Prediction of the Hydration Free Energies of 20 Salts through Adaptive Force Matching and the Proper Comparison with Experimental References. *J. Phys. Chem. B* **2017**, *121,* 6637-6645. (b) Volkov, A. G.; Paula, S. D.; Deamer, W. Two Mechanisms of Permeation of Small Neutral Molecules and Hydrated Ions across Phospholipid Bilayers, *Bioelectrochem Bioenerg* **1997**, *42,* 153-160. (c) Nightingale, E. R. Jr. Phenomenological Theory of Ion Solvation. Effective Radii of Hydrated Ions. *J. Phys. Chem.* **1959**, *63,* 1381-1387.